

Phase structure of spin-imbalanced unitary Fermi gases

I. Boettcher,¹ J. Braun,^{2,3} T. K. Herbst,¹ J. M. Pawłowski,^{1,3} D. Roscher,² and C. Wetterich^{1,3}

¹*Institute for Theoretical Physics, Heidelberg University, D-69120 Heidelberg, Germany*

²*Institut für Kernphysik (Theoriezentrum), Technische Universität Darmstadt, D-64289 Darmstadt, Germany*

³*ExtreMe Matter Institute EMMI, GSI Helmholtzzentrum für Schwerionenforschung mbH, D-64291 Darmstadt, Germany*
(Dated: January 26, 2015)

We investigate the phase structure of spin-imbalanced unitary Fermi gases beyond mean-field theory by means of the Functional Renormalization Group. In this approach, quantum and thermal fluctuations are resolved in a systematic manner. The discretization of the effective potential on a grid allows us to accurately account for both first- and second-order phase transitions that are present on the mean-field level. We compute the full phase diagram in the plane of temperature and spin-imbalance and discuss the existence of other conjectured phases such as the Sarma phase and a precondensation region. In addition, we explain on a qualitative level how we expect that in-situ density images are affected by our findings and which experimental signatures may potentially be used to probe the phase structure.

PACS numbers: 03.75.Ss, 67.85.Lm, 05.10.Cc, 11.10.Hi

I. INTRODUCTION

The ever-growing advances in the experimental probe and control of ultracold quantum gases continuously enrich our understanding of strongly-correlated quantum systems [1]. In particular, the preparation of locally equilibrated many-body systems allows for the exploration of their thermodynamic properties such as the phase structure or the equation of state. Furthermore, the experimental determination of these key observables facilitates the solid benchmarking of theoretical methods for interacting quantum systems.

By populating distinct hyperfine states of a specific class of fermionic atoms (e.g. ^6Li or ^{40}K), it is possible to emulate two- or higher-component fermion systems [2–6] (see Refs. [7, 8] for reviews). This enables the realization of ensembles which are reminiscent of a variety of many-body systems at very different energy scales such as solid state materials or neutron stars and gives us an unprecedented opportunity to study the effects of, e.g., spin-imbalance and temperature in strongly coupled systems [9–13]. The BCS-BEC crossover of two-component fermions close to an atomic Feshbach resonance smoothly interpolates between a superfluid of Cooper pairs and a condensate of composite bosons. In three dimensions, the strongly-coupled unitary Fermi gas (UFG), where the s-wave scattering length diverges, is realized at resonance. Here, the scale for all physical observables is set solely by the Fermi momentum. The high precision in this universal regime on the experimental side opens up the possibility for detailed benchmarks of the large variety of available theoretical methods, such as (Quantum) Monte Carlo calculations [14], ϵ -expansions [15], T -matrix approaches [16], Dyson–Schwinger equations [17], $1/N$ -expansions [18], 2-particle irreducible methods [19], renormalization group flow equations [20–23], ladder resummation techniques [24] and exact as well as universal relations [25].

In conventional superconductors, a sufficiently large

imbalance between spin-up and spin-down electrons destroys superconductivity due to the mismatch of the associated Fermi energies. Such a polarization can be realized in a solid state material by the application of an external magnetic Zeeman field. Since for ultracold atoms the effective spin degree of freedom originates from their individual hyperfine state, this spin-imbalance can be tuned at will by means of a difference in population. In a microscopic model, this manifests itself in a difference in chemical potentials. Hereafter, μ_1 and μ_2 denote the chemical potentials of atoms in state $|1\rangle$ and $|2\rangle$, respectively. We assume the former to be the majority species, i.e. $\mu_1 \geq \mu_2$, without loss of generality.

While the ground state of the spin-balanced UFG is commonly believed to be a homogeneous superfluid, the phase structure in the imbalanced case is less clear. In fact, given $\mu_1 > 0$, the density of minority atoms vanishes for $\mu_2 \lesssim -0.6\mu_1$ [26–33]. This suggests that superfluidity has to break down at a finite critical value of the spin-imbalance. For a BCS superfluid, this already happens for an exponentially small mismatch of Fermi surfaces [34, 35]. However, since the UFG has less pronounced Fermi surfaces, the energy gain from pairing might still compensate the mismatch and hence be energetically favorable. We shall discuss below that within our approximation superfluidity at zero temperature persists down to $\mu_2 \simeq 0.09\mu_1$, where it vanishes at a first-order phase transition.

Besides the breakdown of superfluidity, the existence of exotic phases has been conjectured for the spin-imbalanced UFG. In the mean-field approximation [36–38], the homogeneous Sarma phase [39], a homogeneous superfluid with gapless fermionic excitations, is unstable at zero temperature. This scenario has been found to persist upon inclusion of bosonic fluctuations [40]. Furthermore, inhomogeneous phases such as the Fulde–Ferrell or Larkin–Ovchinnikov-states [41, 42] may be energetically favored over the homogeneous superfluid ground state. Hence, such inhomogeneities have to be taken

into account for a complete study of the phase structure. This, however, is beyond the scope of the present work and we restrict our discussion to homogeneous phases only.

In this work we study the phase structure of the spin-imbalanced three-dimensional UFG beyond the mean-field approximation by means of the Functional Renormalization Group (FRG). This allows us to include the effect of bosonic fluctuations onto the many-body state. Besides a large quantitative improvement, such an analysis of fluctuation effects is also mandatory for a solid understanding of the qualitative features of the phase diagram. In fact, it is known that the mean-field approximation fails to predict the correct order of phase transitions in some cases. In addition, a commonly encountered situation is the suppression of long-range order due to fluctuations of the Goldstone modes which can be captured by our RG approach. Finally, we note that our approach does not suffer from the infamous sign problem which complicates *ab-initio* Monte-Carlo calculations of imbalanced systems. To surmount this problem, new techniques have recently been developed [43, 44] and successfully applied to imbalanced Fermi gases [45]. From this point of view, our present study may also provide useful guidance for future studies of the phase diagram of spin-imbalanced Fermi gases with Monte-Carlo simulations.

This paper is organized as follows: In Sec. II we provide details about our studied system and its phase structure on the mean-field level. Next, we discuss the truncation and numerical implementation of the FRG setup used to include fluctuations beyond the mean-field level. Results on the phase structure of the imbalanced UFG including fluctuations are presented in Sec. IV. We discuss experimental signatures reflecting the phase diagram in Sec. V. Our concluding remarks are given in Sec. VI.

II. MODEL

We consider two-component ultracold fermions close to a broad s-wave Feshbach resonance (FR). The scattering physics can be described by the two-channel model [17, 46], where the closed channel is incorporated by means of a bosonic field ϕ . For a broad FR this is equivalent to a purely fermionic one-channel model: both result in the same universal low-energy physics. In the purely fermionic picture, the bosons emerge as a pairing (or order-parameter) field in the particle-particle channel, $\phi \sim \psi_1 \psi_2$. The assumption of a broad FR is valid, e.g., for ^6Li , where the resonance is located at $B_0 = 832.2\text{ G}$ with a width $\Delta B \simeq 200\text{ G}$ [47].

The microscopic action of the two-channel model reads

$$S[\psi_\sigma, \phi] = \int_X \left[\sum_{\sigma=1,2} \psi_\sigma^* (\partial_\tau - \nabla^2 - \mu_\sigma) \psi_\sigma + \phi^* (\partial_\tau - \nabla^2/2 + \nu_\Lambda) \phi - g(\phi^* \psi_1 \psi_2 + \text{h.c.}) \right]. \quad (1)$$

It serves as the starting point for our computations. The atoms in hyperfine state $|\sigma\rangle$ are represented by a Grassmann-valued field $\psi_\sigma(\tau, \vec{x})$ with imaginary time τ [48, 49]. We employ units such that $\hbar = k_B = 2M = 1$, where M is the mass of the atoms. The imaginary time domain is compactified to a torus of circumference T^{-1} in the standard way and we write $\int_X = \int d\tau \int d^3x$.

We allow for an imbalance in the chemical potentials of the individual species, μ_1 and μ_2 , respectively. Moreover, we assume the 1-atoms to be the majority species such that

$$\delta\mu = h = \frac{\mu_1 - \mu_2}{2} \geq 0, \quad \mu = \frac{\mu_1 + \mu_2}{2}. \quad (2)$$

The spin-imbalance, $\delta\mu$, is frequently also referred to as Zeeman field, h . We can thus write $\mu_{1,2} = \mu \pm \delta\mu$, where μ is the average chemical potential in the system.

The model in Eq. (1) is valid on momentum scales much smaller than a (large) momentum cutoff Λ . In practice one can choose Λ to be sufficiently large compared to the many-body scales determined by density or temperature, but well below the inverse van-der-Waals length. Details of the interatomic interaction are then irrelevant. We further assume the interactions to be of zero range. The detuning from resonance, $\nu_\Lambda \propto (B - B_0)$, has to be fine-tuned such that $a^{-1} = 0$. With this renormalization, thermodynamic observables become independent of Λ and a^{-1} . The Feshbach coupling $g^2 \propto \Delta B$ is related to the width of the resonance, which we assume to be large in the following.

We employ a functional integral representation of the quantum effective action, $\Gamma[\psi_\sigma, \phi]$, in terms of coherent states. The effective action is the generating functional of one-particle irreducible correlation functions. When evaluated at its minimal configuration, it is related to the partition function according to $\Gamma_0 = -\ln Z(\mu, \delta\mu, T)$. For a comprehensive introduction to functional methods in the context of ultracold atoms see, e.g., Refs. [23, 50].

In the present approach, the fermion fields only appear quadratically and can be integrated out, leaving us with a description in terms of the pairing field, ϕ , only. In the BCS-BEC crossover, the pairing field has the intuitive interpretation of Cooper pairs or composite diatomic molecules in the BCS- and BEC-limits, respectively. For the UFG, however, such a simple picture has not been found yet. Loosely speaking, the many-body state in this limit rather is a strongly-correlated quantum soup with both bosonic and fermionic features. We assume the boson field expectation value to be homogeneous in the following, $\phi_0 \neq \phi_0(\vec{x})$. Below we discuss why this should be a reasonable assumption for the spin-imbalanced UFG. A non-vanishing field expectation value $\phi_0(\mu, \delta\mu, T) = \langle \phi \rangle \neq 0$ then signals superfluidity of the system.

The field expectation value is determined by the minimum of the full effective potential,

$$U(\rho = \phi^* \phi) = \Omega^{-1} \Gamma[\phi],$$

where $\Omega = V/T$ with the three-dimensional volume V and $\phi = \text{const.}$ Due to global $U(1)$ -invariance of the microscopic action, the effective potential depends only on the $U(1)$ -invariant $\rho = \phi^* \phi$. Without loss of generality we assume ϕ_0 to be real-valued. For fixed μ and T , the amplitude of ϕ_0 is a (not necessarily strictly) monotonously decreasing function of $\delta\mu$. At the critical imbalance $\delta\mu_c(\mu, T)$, the global minimum of $U(\rho)$ approaches $\rho_0 = 0$ either discontinuously or continuously, resulting in a first- or second-order phase transition, respectively.

In the mean-field approximation the effective action is computed from a saddle-point approximation of the functional integral, here under the assumption of a homogeneous field expectation value. For convenience, we parametrize it in terms of the gap parameter, $\Delta^2 = g^2 \rho$, rather than ρ itself. For the UFG we find

$$U(\Delta^2, \mu, \delta\mu, T) = \int \frac{d^3 q}{(2\pi)^3} \left[(q^2 - \mu - E_q - \frac{\Delta^2}{2q^2}) - T \ln \left(1 + e^{-(E_q - \delta\mu)/T} \right) - T \ln \left(1 + e^{-(E_q + \delta\mu)/T} \right) \right], \quad (3)$$

with $E_q = \sqrt{(q^2 - \mu)^2 + \Delta^2}$, cf. e.g. [36, 38, 51]. The mean-field phase boundary is found from the global minimum, Δ_0^2 , of the effective potential $U(\Delta^2)$. Note that the mean-field approximation can be recovered from the FRG equation when all bosonic fluctuations are neglected, see our discussion below. This allows us to study the impact of fluctuations in a unified approach. We show the mean-field phase diagram in Fig. 1.

The mean-field analysis predicts a first order phase transition at zero temperature at $\delta\mu_c/\mu = 0.807$ (red, solid line). This is often referred to as Chandrasekhar–Clogston limit [34, 35]. At this point, the field expectation value jumps from $\Delta_0/\mu = 1.162$ to zero. The second order phase transition (blue, dashed line) of the balanced case occurs at $T_c/\mu = 0.665$. As a reaction to non-zero spin-imbalance, the transition changes from second to first order at the tricritical point $(\delta\mu_{CP}/\mu, T_{CP}/\mu) = (0.704, 0.373)$ in agreement with previous findings, see Refs. [52, 53] for reviews. Also shown in Fig. 1 are the Sarma crossover (green, dot-dashed line) and so-called preconensation line (black, dotted line). These features are discussed in detail in Sec. IV when we compare the mean-field phase structure to the results from our RG analysis including fluctuations.

III. FUNCTIONAL RENORMALIZATION GROUP

We now include the feedback of bosonic fluctuations onto the effective potential. This is particularly important for the regime with spontaneously broken symmetry, where a massless Goldstone mode appears. The FRG approach allows to systematically include the effect of the

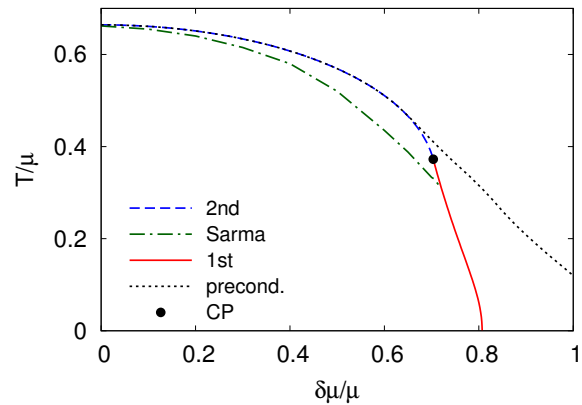


FIG. 1. (Color online) Mean-field phase diagram of the spin-imbalanced UFG. We show the superfluid-to-normal transition and the Sarma crossover. The location of the phase boundaries can be obtained from the mean-field expression for the grand canonical potential, Eq. (3), or from the FRG flow by omitting bosonic fluctuations. In the latter approach it is possible to additionally resolve the preconcentration line (black, dotted line), below which a minimum at $\Delta_{0,k}$ appears during the RG flow, but vanishes for $k \rightarrow 0$, thereby leaving the system in the normal phase. We discuss the phenomenon of preconcentration in Sec. IV in detail.

latter and is free of infrared divergences, see e.g. Refs. [54] for a general introduction to the method, and Refs. [21–23, 55] for an overview on the application in the cold atoms context.

The FRG is based on an exact flow equation for the effective average action $\Gamma_k[\psi_\sigma, \phi]$. The latter interpolates smoothly between the microscopic action at large momentum scales and the full quantum effective action at low momentum scales, $\Gamma_{k=\Lambda} = S$ and $\Gamma_{k=0} = \Gamma$, respectively. Herein k is a flowing momentum scale, and S is given by the microscopic model in Eq. (1) for the present analysis. The flow equation reads

$$\partial_k \Gamma_k[\psi_\sigma, \phi] = \frac{1}{2} \text{STr} \left(\frac{1}{\Gamma_k^{(2)}[\psi_\sigma, \phi] + R_k} \partial_k R_k \right), \quad (4)$$

where $\Gamma_k^{(2)}$ is the second functional derivative with respect to the field content of the theory, and R_k is an infrared regulator [56]. Accordingly, $(\Gamma_k^{(2)} + R_k)^{-1}$ is the full propagator of the regularized theory. STr denotes a supertrace, see e.g. the detailed discussion in [57]. Eq. (4) is an exact equation that is very convenient for practical purposes due to its one-loop structure. However, the presence of the full propagator on the right-hand side makes the use of truncations necessary in most cases of interest.

The effective average action is a functional of the mean-fields, ψ_σ and ϕ , of fermions and bosons, respectively. To approximately resolve its functional form we apply the

ansatz

$$\begin{aligned} \Gamma_k[\psi_\sigma, \phi] = & \int_X \left(\psi_\sigma^* P_{\psi\sigma,k}(\partial_\tau, -i\nabla) \psi_\sigma \right. \\ & + \phi^* P_{\phi,k}(\partial_\tau, -i\nabla) \phi + U_k(\rho = \phi^* \phi) \\ & \left. - g_k(\phi^* \psi_1 \psi_2 + \text{h.c.}) \right). \end{aligned} \quad (5)$$

In this way we parametrize the system in terms of the inverse fermion and boson propagators ($P_{\psi\sigma}$ and P_ϕ), the effective potential (U), and the Feshbach coupling (g). The scheme used in this work builds on a scale-dependent derivative expansion of the boson propagator, while keeping the fermion propagator in its microscopic form. Accordingly, we have

$$P_{\psi\sigma,k}(Q) = P_{\psi\sigma,k}(iq_0, \vec{q}) = iq_0 + q^2 - \mu_\sigma, \quad (6)$$

$$P_{\phi,k}(Q) = P_{\phi,k}(iq_0, \vec{q}) = A_{\phi,k} \left(iq_0 + \frac{q^2}{2} \right). \quad (7)$$

Systematic extensions of this truncation are possible and yield quantitative improvement, see our discussion below and, e.g., [57].

The key ingredient of our analysis is keeping the full functional form of the effective average potential $U_k(\rho)$. In this way we are able to properly resolve first-order phase transitions and also to quantitatively improve results beyond a Taylor expansion of $U_k(\rho)$ in powers of the field. The flow equation for the effective potential is obtained from Eq. (4) for a constant background field ϕ . It is given by

$$\dot{U}_k(\rho) = \dot{U}_k^{(F)}(\rho) + \dot{U}_k^{(B)}(\rho), \quad (8)$$

where the superscripts F and B indicate the contributions from fermionic and bosonic loops, respectively. The dot denotes a derivative with respect to RG-time $t = \ln(k/\Lambda)$. We discuss Eq. (8) in detail in App. A. Here we focus on the most important aspect for the present analysis, which is the interplay between $\dot{U}^{(F)}$ and $\dot{U}^{(B)}$.

The explicit form of the beta function on the right-hand side of Eq. (8) depends on the choice of truncation for Γ_k , and the regulators R_ϕ and $R_{\psi\sigma}$ for bosons and fermions, respectively. To exemplify the key features we now discuss its form obtained for the truncation (5) with the regulators from Eqs. (13) and (15). The general equation is displayed in App. A. For clarity, we restrict the formulas to the zero temperature case for the moment. We then find

$$\begin{aligned} \dot{U}_k^{(F)}(\rho) = & -\frac{k^2}{3\pi^2 \sqrt{1 + g^2 \rho / k^4}} \theta \left(\sqrt{k^4 + g^2 \rho} - \delta \mu \right) \\ & \times \left[(\mu + k^2)^{3/2} \theta(\mu + k^2) - (\mu - k^2)^{3/2} \theta(\mu - k^2) \right] \end{aligned} \quad (9)$$

for the fermionic part, where $\theta(x)$ is the Heaviside step function. There is no direct feedback of $U_k(\rho)$ onto its flow from the expression in Eq. (9). In fact, the integration of only this contribution yields the mean-field effective potential. However, including also bosonic fluctuations has indirect impact on $\dot{U}^{(F)}$ owing to the running Feshbach coupling g_k .

Due to the presence of the bosonic contribution in Eq. (8), we are faced with a coupled flow equation where fermionic and bosonic terms compete. The corresponding flow at zero temperature reads

$$\begin{aligned} \dot{U}_k^{(B)}(\rho) = & \frac{\sqrt{2} k^5}{3\pi^2} \left(1 - \frac{\eta_\phi}{5} \right) \\ & \times \frac{A_\phi k^2 + U'_k(\rho) + \rho U''_k(\rho)}{\sqrt{(A_\phi k^2 + U'_k(\rho))(A_\phi k^2 + U'_k(\rho) + 2\rho U''_k(\rho))}}, \end{aligned} \quad (10)$$

where primes denote derivatives with respect to ρ . The appearance of $U'_k(\rho)$ and $U''_k(\rho)$ on the right-hand side of the flow equation necessitates a good resolution of $U_k(\rho)$ during the flow. For this purpose we discretize the function $U_k(\rho)$ on a grid of typically ≥ 100 points.

The initial condition for the flow of $U_k(\rho)$ is given by $U_\Lambda(\rho) = \nu_\Lambda \rho$. During the flow, the effective average potential acquires a more complex form, which is accounted for by the discretization on the grid. We keep track of the scale-dependent minimum $\rho_{0,k}$, and determine the phase structure from the order parameter $\Delta_0^2 = \Delta_{0,k=0}^2$ at $k = 0$.

The boson dynamics are encoded in the inverse boson propagator P_ϕ , cf. Eq. (7). Here we apply a scale-dependent derivative expansion, where $P_\phi(Q)$ is expanded in powers of iq_0 and q^2 for each scale k separately. Due to the presence of the regulator in the flow equation, this is expected to give a good approximation of the one-loop integral in Eq. (4). We will now argue why the simple form (7) is expected to be sufficient to describe the phase structure. In general, the leading order terms in the expansion of P_ϕ read

$$P_{\phi,k}(Q) = A_{\phi,k} \left(iZ_{\phi,k} q_0 + \frac{1}{2} q^2 + V_{\phi,k} q_0^2 + \dots \right). \quad (11)$$

At the microscopic scale, $A_{\phi,\Lambda} = Z_{\phi,\Lambda} = 1$ and $V_{\phi,\Lambda} = 0$. By taking two functional derivatives of Eq. (4) one can derive the flow equation for P_ϕ , and thus for the running couplings parametrizing it, see e.g. [57].

From studies of bosonic systems it is known that $Z_{\phi,k}$ vanishes like k^{3-d} as $k \rightarrow 0$ in $d < 3$ spatial dimensions, and vanishes logarithmically for $d = 3$ [58–61]. Hence, the linear frequency term is replaced by a quadratic frequency dependence with $V_{\phi,k} > 0$ in the infrared Goldstone regime [59]. In order to describe the boson dynamics consistently, both $Z_{\phi,k}$ and $V_{\phi,k}$ need to be taken into account. Without $V_{\phi,k}$ the propagator at a low scale k would become frequency-independent. However, in three dimensions the running of $Z_{\phi,k}$ with k is only logarithmic, and there is no strict need to incorporate $V_{\phi,k}$. For instance, at the scale k where $\Delta_{0,k}$ saturates, $Z_{\phi,k}$ typically still has a substantial size $\simeq 0.5$, and $V_{\phi,k} q_0^2$ represents a subleading term. Moreover, it has been demonstrated previously that the inclusion of $Z_{\phi,k}$ only leads to corrections of a few percent in, e.g., the critical temperature, cf. [57]. Furthermore, these modifications are counterbalanced to some extent by the running of $V_{\phi,k}$. Hence

we choose the following consistent approximation

$$Z_{\phi,k} = 1, \quad V_{\phi,k} = 0 \quad (12)$$

for all k . The flow of $A_{\phi,k}$, on the other hand, is incorporated by means of the anomalous dimension $\eta_{\phi,k} = -\partial_t \ln A_{\phi,k}$. The corresponding flow equation is given in App. A.

The regulator functions R_ϕ and $R_{\psi\sigma}$ which enter the flow equation (4) have to meet several conditions [54], but can otherwise be chosen freely. If there was no truncation of the effective average action, the fact that the regulator functions vanish for $k \rightarrow 0$ would entail that the result is independent of the regulator. In practice, the truncation introduces a spurious dependence on the choice of regulator, which may be employed for an error estimate by comparing results obtained for different regulators, see e.g. [62].

In order to regularize the fermion propagator we apply two regulator choices separately. They read

$$R_{\psi\sigma}^Q \equiv R_\psi^Q = (k^2 \text{sgn}(\xi_q) - \xi_q) \theta(k^2 - |\xi_q|) \quad (13)$$

and

$$R_{\psi\sigma}^Q = (k^2 \text{sgn}(\xi_{q\sigma}) - \xi_{q\sigma}) \theta(k^2 - |\xi_{q\sigma}|) \quad (14)$$

with $\xi_q = q^2 - \mu$ and $\xi_{q\sigma} = q^2 - \mu_\sigma$, respectively. Both forms regularize only spatial momenta, q^2 , and constitute a generalization of the fermion regulators used for the balanced case in previous works. Remarkably, the choice (13), where both species are regularized around the average chemical potential μ , is sufficient to render all flows finite and furthermore allows to derive analytic flow equations for both $U_k(\rho)$ and $A_{\phi,k}$. In contrast, for the second choice, Eq. (14), the loop integral has to be performed numerically. We find that the resulting phase diagrams for both choices coincide within the numerical error, see App. B.

For the bosons we use

$$\bar{R}_\phi^Q = A_\phi R_\phi^Q = A_\phi (k^2 - q^2/2) \theta(k^2 - q^2/2), \quad (15)$$

as in previous balanced case studies. The full set of flow equations for the running couplings is given in App. A.

We restrict this investigation to the stability of homogeneous superfluid order. A competing effect from inhomogeneous order is expected to show precursors in the renormalization group flow. One of those is the vanishing of $A_{\phi,k}$ at some non-zero momentum scale $k > 0$ [63]. At this point, the truncation employed here would become insufficient. Since we do not detect signs of such a behavior anywhere near the superfluid phase, it seems reasonable to restrict ourselves to a homogeneous order parameter $\Delta_0 \neq \Delta_0(\vec{x})$. A more detailed discussion of the appearance of inhomogeneous order in the presence of spin- and mass-imbalance from an FRG perspective will be given in [64].

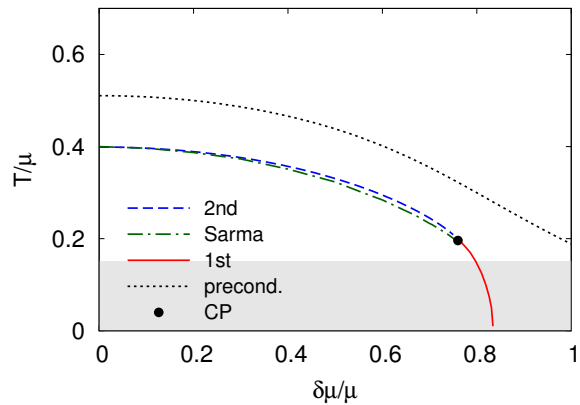


FIG. 2. (Color online) Phase diagram of the spin-imbalanced UFG beyond the mean-field approximation. The phase boundaries are obtained from the FRG evolution of the effective potential including the feedback of bosonic fluctuations. The critical temperature of the balanced system is found to be $T_c/\mu = 0.40$. For small $\delta\mu/\mu$ we find a second order phase transition with a reduced critical temperature. For low temperatures, spin-imbalance results in a breakdown of superfluidity by means of a first-order phase transition. We extract $\delta\mu_c/\mu = 0.83$ for the critical imbalance at zero temperature. The second-order line terminates in a tricritical point (CP). We indicate the Sarma crossover by the green, dash-dotted line. The region between the precondensation line (black, dotted) and the phase boundary gives an estimate for the pseudogap region as is explained in the main text.

IV. RESULTS

We now discuss the phase structure of the system as obtained from the FRG setup described in the previous section. In particular, we show results computed with the fermionic regulator Eq. (13) from above. As we demonstrate in App. B below, these results agree very well with the ones obtained using the regulators Eq. (14), but are numerically more stable due to the analytic expressions for the beta functions.

A. Phase diagram

The phase diagram of the spin-imbalanced UFG beyond mean-field theory is shown in Fig. 2. The overall phase structure is qualitatively similar to the mean-field result, cf. Fig. 1. Noticeably, however, the critical temperature is reduced drastically when fluctuations are included. In the balanced limit we find a second-order phase transition (blue, dashed line) with $T_c/\mu = 0.40$. This is in good agreement with recent measurements [13] as well as QMC calculations [14] and consistent with previous FRG calculations based on a Taylor expansion of the effective potential [57].

As the spin-imbalance is increased, the transition changes from second to first order in a tricritical point

located at $(\delta\mu_{\text{CP}}/\mu, T_{\text{CP}}/\mu) = (0.76, 0.20)$. Below this point we find a first-order transition line, which appears to extend down to $T \approx 0$ (red, solid line). From an extrapolation of the transition line computed for $T \geq 0.01$, we deduce a first-order phase transition for $\delta\mu_c/\mu = 0.83$ at vanishing temperature. This is in reasonable agreement with the recent experimental finding of a first-order transition at $\delta\mu_c/\mu = 0.89$ [65].

Notably, the critical imbalance at zero temperature lies above the mean-field value ($\delta\mu_c^{\text{MFA}}/\mu = 0.807$). This is an interesting observation since usually bosonic fluctuations tend to destroy ordering. In the present case, however, the non-trivial feedback of those fluctuations into the flow also modifies the fermionic “mean-field” contributions from $\dot{U}_k^{(F)}$. In this way, for large enough $\delta\mu$ and small enough T , the non-trivial minimum of U_k is stabilized rather than washed out. This illustrates how the competition of fermionic and bosonic contributions results in non-trivial effects on the phase structure of the system. Unfortunately, the nonlinear structure of the FRG flow equations inhibits a straightforward interpretation of these observations in terms of customary many-body phenomenology. A more detailed investigation in this respect is left for future work.

Note that it is numerically impossible to calculate observables at exactly $k = 0$. However, the flow usually freezes out at a finite scale below the relevant many-body scales present in the theory. In order to reliably extract the phase structure we may hence stop the integration of the flow equation at any sufficiently small k such that $\Delta_{0,k} \simeq \Delta_{0,k=0}$ is frozen out. Especially in the first-order region at low temperatures $T/\mu \lesssim 0.15$, the complexity of the flow equation makes it harder to reach the deep infrared. Due to accumulating numerical errors, the flow needs to be stopped at relatively high $k < 1$. This entails that a sufficient convergence of $\Delta_{0,k}$ inside the superfluid phase might not be achieved yet. However, we will argue in Sec. IV B below that the position of the first-order phase transition is not affected and can still be determined accurately. A conservative estimate of the domain where the IR scale is modified is indicated by the gray band in Fig. 2.

Concerning the regulator dependence, we find the result for the phase boundary to differ by less than 5% for the two choices of fermion regulators in Eqs. (13) and (14). We compare both phase diagrams in Fig. 5 and provide a more detailed discussion in App. B. The insensitivity of the critical line to the regularization scheme indicates the stability of our predictions within the given truncation scheme for the effective average action. We would also like to note here that, at least for small spin imbalances, one may employ a Taylor expansion for the effective potential $U(\rho)$ as recently done in Ref. [66]. At least for an expansion up to order ρ^2 we observe that the results for the critical temperature from a Taylor expansion of the effective potential are larger than those from our study with a discretized effective potential, which naturally includes higher-order couplings. More-

over, the difference between the critical temperatures increases with increasing spin-imbalance, see Fig. 6 in App. B for a more detailed discussion.

In addition to the superfluid-to-normal transition we also show the crossover to the so-called Sarma phase [39], which we determine from the criterion $0 < \Delta_0 \leq \delta\mu$. If the latter condition is fulfilled, the lower branch of the dispersion of fermionic quasiparticles,

$$E_p = \sqrt{(p^2 - \mu)^2 + \Delta_0^2} - \delta\mu, \quad (16)$$

extends below zero. Strictly speaking, the Sarma phase is well defined only for $T = 0$ where one finds a momentum interval $[p_{\text{min}}, p_{\text{max}}]$ which is occupied macroscopically. In turn, this also results in gapless fermionic excitations in the homogeneous superfluid. For an extended discussion of the Sarma phase in the BCS-BEC crossover we refer to [40, 53].

Already on the mean-field level the Sarma phase is found to be absent at low T . The Sarma crossover meets the first order transition line just below the critical point. For lower temperatures, the Sarma criterion cannot be fulfilled anymore since the gap jumps to zero from $\Delta_0 > \delta\mu_c$. This situation persists beyond the mean-field level, as can be seen in Fig. 2. In fact, the Sarma phase shrinks at low imbalance, occurring only in the close vicinity of the superfluid-to-normal transition. Interestingly, the opposite effect has been observed on the BCS side of the crossover in two spatial dimensions: there it is found that the inclusion of bosonic fluctuations beyond mean-field theory changes the transition from first to second order, entailing the presence of a Sarma phase even at $T = 0$, see Ref. [67].

B. Scale evolution and precondensation

In Fig. 3 we show the scale evolution of the minimum of the effective average potential as a function of the RG-scale k for fixed $T/\mu = 0.17$ and two different spin-imbalances, $\delta\mu_{\text{SF}} = 0.78\mu$ and $\delta\mu_{\text{NF}} = 0.79\mu$. For large k the running of couplings is attracted to an ultraviolet fixed point. This scaling regime is left when k becomes of the order of the many-body scales, see App. A. For low enough temperatures local symmetry breaking occurs at $k^2 \simeq \mu$, associated with a non-zero minimum of the effective potential, $\Delta_{0,k} > 0$. Competing bosonic and fermionic fluctuations then determine whether the non-vanishing gap remains (red, solid line) or vanishes (blue, dotted line) in the infrared (IR), i.e. for $k \rightarrow 0$.

The two values of $\delta\mu$ shown in Fig. 3 are chosen such that they lie on the opposite sides of the first-order phase boundary. In both cases a non-vanishing gap, $\Delta_{0,k} > 0$, is generated during the flow at t_{sb} . Only for $\delta\mu = \delta\mu_{\text{SF}}$ it persists for $t \rightarrow -\infty$, leading to superfluidity (SF) and symmetry breaking in the IR. For $\delta\mu = \delta\mu_{\text{NF}}$ instead, $\Delta_{0,k}$ jumps back to zero at the finite scale $t_{\text{sr}} = -7.69$, below which the symmetry remains restored such that

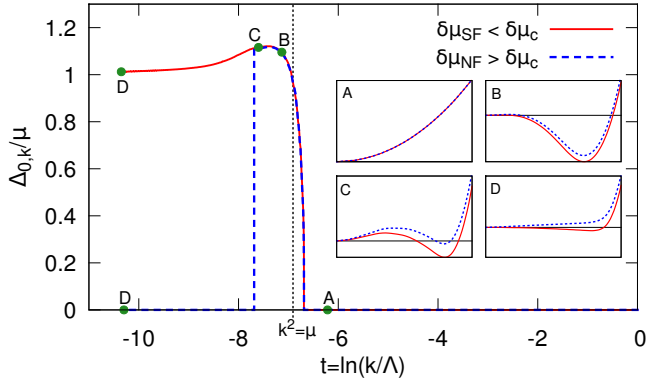


FIG. 3. (Color online) Scale evolution of the minimum $\Delta_{0,k}$ of the effective average potential close to a first-order phase transition at $\delta\mu_c$. The evolution proceeds from the ultraviolet ($k = \Lambda$, $t = 0$) to the infrared ($k \rightarrow 0$, $t \rightarrow -\infty$). The insets show the shape of the effective potential $U_k(\Delta)$ at several points along the scale evolution. The solid (red) lines correspond to a point in the broken phase ($\delta\mu_{SF} = 0.78\mu$), where the global minimum of the effective potential is non-zero in the infrared. The dotted (blue) line represents a point with $\delta\mu_{NF} = 0.79\mu$, where the global minimum in the infrared is located at $\Delta_{0,k=0} = 0$. For all plots, $T/\mu = 0.17$.

one finds a normal fluid (NF). In both cases, the effective potential at intermediate k exhibits two local minima (inset C), but for $\delta\mu_{NF}$ the non-trivial one is raised above $U_k(\rho = 0)$ and disappears (inset D) during the flow.

The appearance of a non-zero $\Delta_{0,k}$ in a limited range $k_{sr} < k < k_{sb}$ is called *precondensation*, see e.g. [23]. It can be interpreted as the formation of pairs and local phase coherence, although long-range order is destroyed due to fluctuations. The associated coherence length can be estimated by k_{sr}^{-1} . An analogous phenomenon exists in relativistic theories [68]. In Fig. 2 the precondensation region is enclosed by the black, dotted line and the phase boundary.

The phenomenon of precondensation is closely related to pseudogap physics, which refers to a situation where the gas is in the normal phase, although low-lying fermionic excitations are gapped. We refer to [69, 70] for a discussion of the latter in the context of superconductivity, and [71–74] for pseudogap physics in ultracold Fermi gases. In our case, superfluidity is absent due to $\Delta_0 = 0$, but excitations with momentum $k_{sr} < k < k_{sb}$, which is typically on the order of k_F , are energetically disfavoured. This leads to a strong suppression in the density of states and thus of the contribution of these modes to the many-body properties of the system. For instance, a common experimental signature for both pseudogap and precondensation phenomena would be a suppression of entropy above the critical temperature compared to the high temperature limit. Radio-frequency spectroscopy allows to deduce the pseudogap regime from the spectral function of cold atomic gases. With this method a pseudogap regime above the criti-

cal temperature has indeed been observed for the UFG [71, 72, 74].

Moreover, we compare our finding for the precondensation temperature in the balanced case, $T_{pc}/\mu = 0.51$, to analogous values obtained with other methods. A suppression of the entropy above the critical temperature, and thus a deviation of the specific heat from the normal gas expectation, is reported in Ref. [14] below $T_0/\mu = 0.55(5)$. From the above consideration on the entropy we conclude that this constitutes an estimate for T_{pc} , which is in good agreement with our result. Our value $T_{pc}/T_c = 1.25$ is also in line with the results in [75, 76] from a T-matrix approach, where different definitions of the pseudogap have been distinguished.

For vanishing or small spin-imbalance, $\Delta_{0,k}$ approaches zero continuously in the precondensation region, see e.g. Fig. 28 in Ref. [23]. For configurations with large $\delta\mu/\mu$ and low T/μ as in Fig. 3, a jump of $\Delta_{0,k}$ can be observed instead. This behavior is only possible in the vicinity of a first-order phase transition. It is generated by a second, non-trivial local minimum of the effective potential which is raised above $U_k(\rho = 0)$ during the flow (cf. insets C and D). An interesting consequence is that this type of precondensation is not necessarily induced by bosonic fluctuations alone. In fact, even in the mean-field approximation, where the latter are absent, we find a pseudogap regime for large $\delta\mu/\mu$, see Fig. 1.

Furthermore, the peculiar k -dependence of the gap at the first-order transition region can be exploited numerically. A smooth decrease to zero of $\Delta_{0,k}$, as occurring close to a second-order phase transition, may take arbitrarily long in RG-time. Therefore, an IR scale of about $t \approx -11$ should be considered as an upper limit for the reliable extraction of results for finite $\Delta_{0,k=0}$. However, for $T/\mu \leq 0.15$ (shaded area in Fig. 2), $t \approx -9$ is often the utmost that can be reached, due to the increasing stiffness of the flow equations. Thus, the estimate for the value of $\Delta_{0,k=0} > 0$ in the superfluid phase is less reliable for such low temperatures. In contrast, the position of the first-order phase transition is determined by the occurrence of a sudden breakdown of the condensate. Indeed, we find that this jump to $\Delta_{0,k} = 0$ always occurs at some $t > -8$ for $T/\mu \leq 0.15$. Since these scales are not affected by the IR problems mentioned above, we conclude that our results for the position of the phase transition can be trusted even in the shaded area.

As a final remark, we mention that the scale evolution of $U_k(\rho)$ as shown in Fig. 3 allows to check the quality and consistency of truncation, regularization and initial conditions. For example, it can be seen in inset D that the FRG-evolved effective potential is convex for $k \rightarrow 0$ within our truncation, cf. [77]. This exact property is reproduced by FRG flows [54, 78]. It can, however, be spoiled by an insufficient truncation. The mean-field approximation, for instance, is included in the FRG equation as a truncation that neglects all bosonic contributions, cf. our discussion above. However, the mean-field effective potential is non-convex in the infrared.

V. EXPERIMENTAL SIGNATURES

Our findings on the phase structure of the spin-imbalanced UFG have immediate consequences on the qualitative shape of in-situ density profiles, $n(\vec{r})$, obtained for this system in experiment. Here, we briefly recapitulate the phenomenology of second- and first order phase transitions in an external potential, and also discuss the impact of the precondensation region on the interpretation of experimental results. To this end, we define the density and population imbalance by

$$n(\mu, \delta\mu, T) = n_1 + n_2 = \left(\frac{\partial P}{\partial \mu} \right)_{\delta\mu, T}, \quad (17)$$

$$\delta n(\mu, \delta\mu, T) = n_1 - n_2 = \left(\frac{\partial P}{\partial \delta\mu} \right)_{\mu, T}, \quad (18)$$

respectively. Here, P is the pressure, and n_σ is the density of atoms in hyperfine state $|\sigma\rangle$.

For an ultracold quantum gas confined to an external trapping potential $V(\vec{r})$, the thermodynamic equilibrium state depends on the particular shape of the trap. In many cases, however, we can apply the local density approximation (LDA), which assigns a local chemical potential $\mu(\vec{r}) = \mu_0 - V(\vec{r})$ to each point in the trap. Here μ_0 is the central chemical potential. In this way, thermodynamic observables computed for the homogeneous system are translated into those of the trapped system. Note that T and $\delta\mu$ are assumed to be constant throughout the trap within the LDA. The LDA can be applied if the length scale ℓ_0 associated to the trap is much larger than all other scales of the many-body system. For instance, in a harmonic trap, $V(\vec{r}) = M\omega_0^2 r^2/2$, the former scale is given by the oscillator length $\ell_0 = \sqrt{\hbar/M\omega_0}$. The many-body length scales of the UFG are given by $k_F^{-1} \propto (2M\mu/\hbar^2)^{-1/2}$, $(2M\delta\mu/\hbar^2)^{-1/2}$, and $\lambda_T = (Mk_B T/2\pi\hbar^2)^{-1/2}$, respectively. Often the LDA is a good approximation for sufficiently high densities. However, it breaks down in the outer regions of the trap, where the gas is extremely dilute, and close to a second order phase transition, where the correlation length diverges (and thus becomes larger than ℓ_0).

If the central chemical potential, μ_0 , is sufficiently larger than T , the inner region of the trapped system is superfluid. Above a certain critical radius, r_c , the superfluid core vanishes and is replaced by a quantum gas in the normal phase. The critical radius is related to the critical chemical potential, $\mu_c(T, \delta\mu)$, according to $\mu_c = \mu_0 - V(\vec{r}_c)$. At a first-order phase transition, the density at μ_c exhibits a jump. Accordingly, the superfluid inner region and the normal region are separated by a jump in the density at r_c . We sketch this in Fig. 4. In contrast, the transition is continuous for a second-order phase transition. In this way, the order of the phase transition, and our prediction for the temperature of the tricritical point, $T_{CP}/\mu_0 = 0.20$, may potentially be verified from in-situ images at different temperatures.

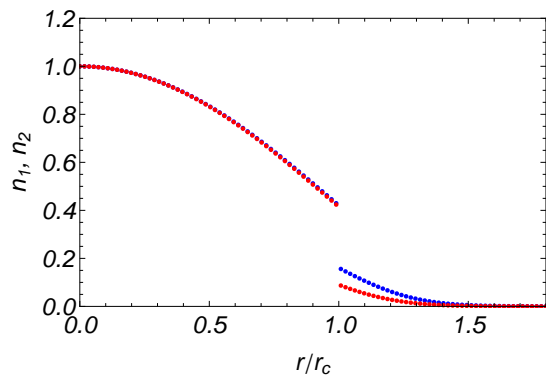


FIG. 4. (Color online) Schematic in-situ density profile $n_\sigma(r)$ for a population-imbalanced ensemble with $N_1 > N_2$ at low temperature. The blue and red points correspond to atoms in hyperfine state $|1\rangle$ and $|2\rangle$, respectively. For $T < T_{CP}$ the superfluid transition is of first order, such that the superfluid inner region is separated from the polarized normal gas by a jump in density at the critical radius r_c .

In experiments with cold atoms, the imbalance between spin-partners is introduced by different atom numbers $N_1 \geq N_2$ for atoms in state $|1\rangle$ and $|2\rangle$, respectively. The influence of a non-zero polarization $p = (N_1 - N_2) / (N_1 + N_2)$ is very distinct for trapped systems in comparison to homogeneous ones [79–81]. For a *trapped system*, the particle numbers N_σ are obtained from an integral over the whole cloud, $N_\sigma = \int_{\vec{r}} n_\sigma(\vec{r})$. As a consequence, phase separation takes place in real space by means of a superfluid core and a surrounding normal region. Both are separated by the above-mentioned jump in the density.

With a state-resolved detection of individual densities, $n_1(\vec{r})$ and $n_2(\vec{r})$, it is possible to measure the local in-situ polarization $p(\vec{r})$ of the trapped gas. According to our finding that there is no Sarma phase at zero temperature, a non-zero polarization inside the superfluid core of the cloud can only be detected at $T > 0$ [40]. As we find the Sarma phase only to appear at very high temperatures and close to the phase boundary, a substantial local polarization $p(\vec{r})$ of the superfluid should only be detectable for $r \lesssim r_c$.

To mimic the effect of a trap potential in our RG study, one may consider the length scale ℓ_0 associated with a trap as an infrared cutoff, $k_f \sim \ell_0^{-1}$. In fact, in a harmonic oscillator potential, the energy of the one-particle states is bounded from below by the oscillator frequency ω_0 . Due to the presence of this infrared scale, long-range fluctuations are cut off. In a first attempt of simulating trap effects, one may therefore identify the infrared cutoff k_f with ℓ_0^{-1} and stop the RG flow at this scale. However, despite being intuitively reasonable, the relation $k_f = \ell_0^{-1}$ has to be taken with some care and can at best give qualitative insights [82–84].

In our analysis we find a substantial precondensation region in the phase diagram, Fig. 2, where a minimum $\rho_{0,k} > 0$ appears during the flow, but is eventually

washed out such that $\rho_0 = \rho_{0,k=0} = 0$. The restoration of symmetry is due to long wavelength fluctuations on length scales $k^{-1} \rightarrow \infty$. However, if long wavelength fluctuations are cut off by a trap with scale ℓ_0 , a superfluid order parameter $\rho_0 \approx \rho_{0,k=k_f}$ can be observed experimentally even in the precondensation phase.

As discussed in Sec. IV B, the first-order transition is barely influenced by the final scale k_f , as long as the latter is below the relevant many-body scales. Therefore, it may be possible to detect the first-order transition and its location even in a trap. On the other hand, for smaller spin-imbalance, where the transition is of second order, this effect can be substantial. As a consequence, we expect that the second-order phase boundary of the homogeneous system is likely to be overestimated by applying the LDA to a trapped gas.

VI. CONCLUSION AND OUTLOOK

In this work we have discussed the phase structure of the spin-imbalanced unitary Fermi gas as obtained from an FRG study. This method presents a tool to study the impact of fluctuations in a systematic manner. In particular, there is a truncation that is equivalent to the standard saddle-point (mean-field) approximation. From this starting point, we have additionally included order-parameter fluctuations that are missing in mean-field theory.

Technically, the discretization of the effective potential on a grid allows us to resolve multiple local minima and therefore it opens up the possibility to reliably determine first-order phase transitions. Moreover, the full functional form of the effective potential is included in such an approach.

Our results show that the qualitative phase structure persists beyond mean-field theory: There is a second-order phase transition in the balanced case that changes to first order in a tricritical point at finite imbalance. At vanishing temperature, superfluidity breaks down in a first-order transition. Quantitatively, however, the influence of bosonic fluctuations is more drastic: in the balanced case, the critical temperature is lowered from $T_{\text{MF}}/\mu = 0.665$ to $T_{\text{FRG}}/\mu = 0.40$, in good agreement with other theoretical predictions [57], QMC calculations [14] and experimental results [13]. At $T = 0$ we find that fluctuations enhance the critical imbalance in comparison to the mean-field value. This, again, is in line with recent experiments [65].

Furthermore, the FRG provides access to the full scale-evolution of observables, from microscopic to macroscopic scales. This puts us in the position to discuss the physics of precondensation, which is related to the formation of a condensate at intermediate scales k . Interestingly, already in the mean-field approximation we find a precondensation temperature that is significantly higher than the critical temperature at high imbalance. This suggests that the formation of a pseudogap is not

solely triggered by order-parameter fluctuations. Beyond the mean-field level, the precondensation temperature is substantially above the critical one throughout the whole phase diagram.

Building on the framework presented here, several interesting directions can be pursued in the future: For example, it has been conjectured that the UFG might feature more exotic phase, such as Sarma [37, 39, 40, 53] and/or inhomogeneous (FFLO) phases [41, 42, 53, 64, 85–87]. Furthermore, the study of mass-imbalance is possible in a similar theoretical fashion [64] and has gained experimental interest recently.

While the UFG is an interesting system that features strong correlations, our approach is not confined to this setting. The inclusion of finite inverse scattering lengths is straight-forward and the imbalanced BCS-BEC crossover is accessible [40]. Moreover, the extension of our approach to the two-dimensional BCS-BEC crossover is straight-forward. In the latter case, the importance of a grid-solution for the effective potential is even more pronounced due to the vanishing canonical dimension of the boson field in two dimensions.

Acknowledgements

I.B., T.K.H., J.M.P., C.W. thank N. Strodthoff and L. von Smekal for valuable discussions and collaboration on related projects. I.B. acknowledges funding from the Graduate Academy Heidelberg. This work is supported by the Helmholtz Alliance HA216/EMMI and the ERC advanced grant 290623. J.B. and D.R. thank J. E. Drut for collaboration on related projects and acknowledge support by the DFG under Grant BR 4005/2-1 and by HIC for FAIR within the LOEWE program of the State of Hesse.

Appendix A: Flow equations

In this appendix we derive the flow equations for the effective potential and the boson anomalous dimensions in the spin-imbalanced UFG. The expressions are given in general form (for frequency- and momentum-independent vertices), and then specialized to our particular choice of truncation and regularization scheme. In order to simplify the comparison to previous works on the FRG approach to the BCS-BEC crossover we remark here that we derive the flow equations for the unrenormalized couplings only. The latter are often displayed with an overbar, which we omit here.

The regularized fermion propagator with respect to the field $(\psi_1, \psi_2, \psi_1^*, \psi_2^*)$ in our truncation reads

$$G_\psi(Q) = \frac{1}{\det_{F12}^Q \det_{F12}^{-Q}} \begin{pmatrix} A & B \\ C & D \end{pmatrix} \quad (\text{A1})$$

with

$$A = g\phi \begin{pmatrix} 0 & \det_{F12}^Q \\ -\det_{F12}^{-Q} & 0 \end{pmatrix}, \quad (\text{A2})$$

$$B = \begin{pmatrix} L_{\psi 2}^{-Q} \det_{F12}^Q & 0 \\ 0 & L_{\psi 1}^{-Q} \det_{F12}^{-Q} \end{pmatrix}, \quad (\text{A3})$$

$$C = \begin{pmatrix} -L_{\psi 2}^Q \det_{F12}^{-Q} & 0 \\ 0 & -L_{\psi 1}^Q \det_{F12}^Q \end{pmatrix}, \quad (\text{A4})$$

$$D = g\phi \begin{pmatrix} 0 & -\det_{F12}^{-Q} \\ \det_{F12}^Q & 0 \end{pmatrix}. \quad (\text{A5})$$

We denote $L_{\psi\sigma}^Q = P_{\psi}(Q) + R_{\psi\sigma}^Q$ and $\det_{F12}^Q = L_{\psi 1}^{-Q} L_{\psi 2}^Q + g^2 \rho$. For the fermion regulator we insert either Eq. (13) or (14). The regulator matrix reads

$$R_{\psi}(Q) = \begin{pmatrix} 0 & 0 & -R_{\psi 1}^{-Q} & 0 \\ 0 & 0 & 0 & -R_{\psi 2}^{-Q} \\ R_{\psi 1}^Q & 0 & 0 & 0 \\ 0 & R_{\psi 2}^Q & 0 & 0 \end{pmatrix}. \quad (\text{A6})$$

The resulting contribution to the flow of the effective potential is given by

$$\dot{U}^{(F)}(\rho) = -\frac{1}{2} \text{Tr} \left(G_{\psi} \dot{R}_{\psi} \right) = - \int_Q \frac{L_{\psi 1}^{-Q} \dot{R}_{\psi 2}^Q + L_{\psi 2}^Q \dot{R}_{\psi 1}^{-Q}}{\det_{F12}^Q}. \quad (\text{A7})$$

The regularized boson propagator in the conjugate field basis, (ϕ, ϕ^*) , is given by

$$G_{\phi}(Q) = \frac{1}{\det_B(Q)} \begin{pmatrix} -\rho U''(\rho) & L_{\phi}^{-Q} \\ L_{\phi}^Q & -\rho U''(\rho) \end{pmatrix}, \quad (\text{A8})$$

with $L_{\phi}^Q = P_{\phi}(Q) + R_{\phi}^Q + U'(\rho) + \rho U''(\rho)$ and $\det_B^Q = L_{\phi}^{-Q} L_{\phi}^Q - (\rho U''(\rho))^2$. The corresponding regulator matrix reads

$$\bar{R}_{\phi}(Q) = \begin{pmatrix} 0 & \bar{R}_{\phi}^{-Q} \\ \bar{R}_{\phi}^Q & 0 \end{pmatrix}. \quad (\text{A9})$$

We arrive at

$$\dot{U}^{(B)}(\rho) = \frac{1}{2} \text{Tr} \left(G_{\phi} \dot{R}_{\phi} \right) = \frac{1}{2} \int_Q \frac{L_{\phi}^Q \dot{\bar{R}}_{\phi}^{-Q} + L_{\phi}^{-Q} \dot{\bar{R}}_{\phi}^Q}{\det_B^Q} \quad (\text{A10})$$

for the bosonic contribution to the flow of the effective potential.

We project the flow of the gradient coefficient A_{ϕ} from the $\phi_2 \phi_2$ -component of the inverse boson propagator, i.e. we have

$$\eta_{\phi} = - \frac{1}{A_{\phi}} \frac{\partial^2}{\partial p^2} \dot{G}_{\phi,22}^{-1}(P) \Big|_{P=0, \rho=\rho_0, k}, \quad (\text{A11})$$

where $(\delta^2 \Gamma[\phi] / \delta \phi_2 \delta \phi_2)(Q, Q') = G_{\phi,22}^{-1}(Q) \delta(Q - Q')$, see e.g. [57]. In the following we assume regulators which do not depend on the frequency, $R^Q = R(q^2)$, but the derivation can also be performed for Q -dependent regulators. We define

$$R^x(q^2) = \frac{\partial R}{\partial q^2}(q^2), \quad R^{xx}(q^2) = \frac{\partial R^x}{\partial q^2}(q^2). \quad (\text{A12})$$

We then find $\eta_{\phi} = \eta_{\phi}^{(F)} + \eta_{\phi}^{(B)}$ with

$$\begin{aligned} \eta_{\phi}^{(F)} = & 2A_{\phi} g^2 \int_Q \left(\frac{\dot{R}_{\psi 1}(1 + R_{\psi 2}^x + 2q^2 R_{\psi 2}^{xx}/d)}{(\det_{F12}^Q)^2} \right. \\ & + \frac{\dot{R}_{\psi 2}(1 + R_{\psi 1}^x + 2q^2 R_{\psi 1}^{xx}/d)}{(\det_{F12}^Q)^2} - \frac{4q^2/d}{\det_{F12}^Q} \\ & \left. \times \left[\dot{R}_{\psi 1} L_{\psi 1}^{-Q} (1 + R_{\psi 2}^x)^2 + \dot{R}_{\psi 2} L_{\psi 2}^Q (1 + R_{\psi 1}^x)^2 \right] \right), \end{aligned} \quad (\text{A13})$$

and

$$\begin{aligned} \eta_{\phi}^{(B)} = & 4A_{\phi} \rho (U'')^2 \int_Q \dot{R}_{\phi}(q^2) \left(\frac{1 + 2R_{\phi}^x + 4q^2 R_{\phi}^{xx}/d}{\det_B^2(Q)} \right. \\ & \left. - \frac{2q^2(1 + 2R_{\phi}^x)^2 L_{\phi}^S(Q)/(A_{\phi} d)}{\det_B^3(Q)} \right). \end{aligned} \quad (\text{A14})$$

In the last line we have introduced the symmetric component $L_{\phi}^S(Q) = (L_{\phi}^Q + L_{\phi}^{-Q})/2$ and employed $d = 3$. Note that in order to evaluate the integrals it is convenient to smear out the step functions $\theta(x)$ in the regulators, e.g. $\theta_{\varepsilon}(x) = (e^{-x/\varepsilon} + 1)^{-1}$ with small $\varepsilon > 0$.

For large $k \lesssim \Lambda$ the running of couplings is attracted to an approximate ultraviolet fixed point where $\eta_{\phi} = 1$ [21, 57]. To simplify the early stage of the flow we start at the fixed point solution. This corresponds to the initial values

$$g_{\Lambda}^2 = 6\pi^2 \Lambda, \quad \nu_{\Lambda} = \Lambda^2 \quad (\text{A15})$$

within our truncation and regularization scheme. The value for ν_{Λ} is fine-tuned such that the resonance condition, $a^{-1} = 0$, is fulfilled. The couplings start to deviate from the ultraviolet fixed point once the flow parameter reaches the many-body scales, i.e. $k^2 \simeq \mu, T, \delta\mu$. We choose $\mu/\Lambda^2 = 10^{-6}$, which is sufficient to suppress the contributions of many-body effects to the early stages of the flow. The scale $k^2 = \mu$ then corresponds to an RG-time $t = \ln(\sqrt{\mu}/\Lambda) = -6.9$.

For the optimized cutoffs employed in this work, an overall $\dot{R}_{\psi\sigma}$ (\dot{R}_{ϕ}) implies that $1 + R_{\psi\sigma}^x \equiv 0$ ($1 + 2R_{\phi}^x \equiv 0$) in the integral. Accordingly, we find

$$\eta_{\phi}^{(B)} = \frac{16A_{\phi} \rho (U'')^2}{d} \int_Q \dot{R}_{\phi}(q^2) \frac{q^2 R_{\phi}^{xx}}{\det_B^2(Q)} \quad (\text{A16})$$

for the bosonic contribution to the anomalous dimension. For the fermionic contribution the simplification only occurs with the choice $R_{\psi 1} = R_{\psi 2} = R_{\psi}$ with R_{ψ} from

Eq. (13). In this case we arrive at

$$\eta_\phi^{(F)} = \frac{8A_\phi g^2}{d} \int_Q \dot{R}_\psi \frac{q^2 R_\psi^{\text{xx}}}{(\det_1^Q)^2}. \quad (\text{A17})$$

The flow equations for the effective potential and the boson anomalous dimension can be expressed in closed analytic form for the choice of cutoffs $R_{\psi 1} = R_{\psi 2} = R_\psi$ from Eq. (13) and R_ϕ from Eq. (15). We then find

$$\begin{aligned} \dot{U}^{(F)}(\rho) = & -\frac{8v_d k^{d+2}}{d\sqrt{1+w_3}} \ell_u(\tilde{\mu}) \left(1 - N_F(\sqrt{1+w_3} - \delta\tilde{\mu}) \right. \\ & \left. - N_F(\sqrt{1+w_3} + \delta\tilde{\mu}) \right) \end{aligned} \quad (\text{A18})$$

and

$$\begin{aligned} \dot{U}^{(B)}(\rho) = & \frac{4v_d 2^{d/2} k^{d+2}}{d} \left(1 - \frac{\eta_\phi}{d+2}\right) \frac{2+w_1+w_2}{\sqrt{(1+w_1)(1+w_2)}} \\ & \times \left(\frac{1}{2} + N_B(\sqrt{(1+w_1)(1+w_2)})\right) \end{aligned} \quad (\text{A19})$$

with $\delta\tilde{\mu} = \delta\mu/k^2$ and

$$w_1 = \frac{U'_k(\rho)}{A_\phi k^2}, \quad w_2 = \frac{U'_k(\rho) + 2\rho U''_k(\rho)}{A_\phi k^2}, \quad w_3 = \frac{g^2 \rho}{k^4}. \quad (\text{A20})$$

We define $v_d = [2^{d+1} \pi^{d/2} \Gamma(d/2)]^{-1}$, and

$$N_F(z) = \frac{1}{e^{k^2 z/T} + 1}, \quad N_B(z) = \frac{1}{e^{k^2 z/T} - 1} \quad (\text{A21})$$

with $N'_{F/B}(z) = \partial_z N_{F/B}(z)$, and

$$\begin{aligned} \ell_u(x) &= \theta(x+1)(x+1)^{d/2} - \theta(x-1)(x-1)^{d/2}, \quad (\text{A22}) \\ \ell_\eta(x) &= \theta(x+1)(x+1)^{d/2} + \theta(x-1)(x-1)^{d/2}. \end{aligned} \quad (\text{A23})$$

The contributions to the anomalous dimension read

$$\begin{aligned} \eta_\phi^{(F)} = & \frac{4v_d A_\phi g^2 k^{d-4}}{d(1+w_3)^{3/2}} \ell_\eta(\tilde{\mu}) \left[\left(1 - N_F(\sqrt{1+w_3} - \delta\tilde{\mu}) \right. \right. \\ & \left. \left. - N_F(\sqrt{1+w_3} + \delta\tilde{\mu}) \right) \right. \\ & \left. + \sqrt{1+w_3} \left(N'_F(\sqrt{1+w_3} - \delta\tilde{\mu}) \right. \right. \\ & \left. \left. + N'_F(\sqrt{1+w_3} + \delta\tilde{\mu}) \right) \right] \end{aligned} \quad (\text{A24})$$

and

$$\begin{aligned} \eta_\phi^{(B)} = & \frac{8v_d 2^{d/2} A_\phi \rho_0 (U'')^2 k^{d-4}}{d[(1+w_1)(1+w_2)]^{3/2}} \\ & \times \left(\frac{1}{2} + N_B(\sqrt{(1+w_1)(1+w_2)})\right) \\ & - \sqrt{(1+w_1)(1+w_2)} N'_B(\sqrt{(1+w_1)(1+w_2)}) \end{aligned} \quad (\text{A25})$$

In the expressions for η_ϕ we evaluate the beta functions for $\rho = \rho_{0,k}$. In the balanced limit, where $\delta\tilde{\mu} = 0$, we recover the flow equations given in Ref. [21].

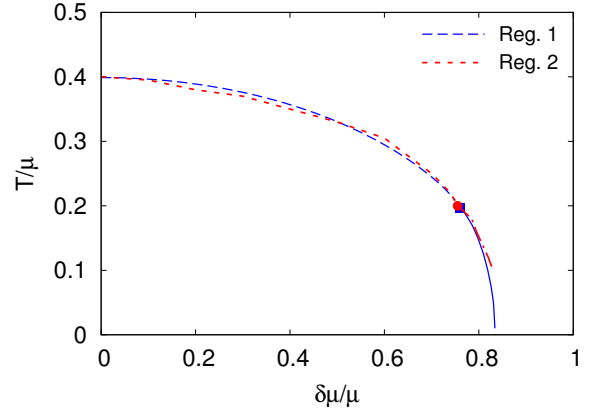


FIG. 5. (Color online) Regularization scheme dependence of the phase boundary. We display the phase diagram obtained by applying the fermion regulator $R_{\psi\sigma}$ from Eqs. (13) (blue long-dashed, “Reg. 1”) and (14) (red short-dashed, “Reg. 2”).

Appendix B: Stability of the phase structure

Here we discuss the stability of the FRG phase structure with respect to the choice of regulator as well as a different expansion of the flow equation.

As we have discussed in the main text, without truncations to the flow equations, all permissible regulators should reproduce the same physics in the IR. In practice, however, one has to resort to truncations as well as stop the flow at a finite, if low, infrared scale. This entails that the strict regulator-independence is lost. However, for a stable truncation, differences should be small. This is what we demonstrate in Fig. 5: The blue (solid and dashed) lines show the superfluid-to-normal transition in the second- and first-order region, obtained with the regulator Eq. (13). The location of the tricritical point is also indicated. The red (short-dashed and dot-dashed) lines show the same for regulator Eq. (14). As can be seen, the two lines lie close to each other throughout the whole phase diagram. Deviations in the critical temperature are below 5% and we mostly attribute them to the presence of numerical integrals with Eq. (14). Hence we can safely claim that our results are stable with respect to a change in the regulator function.

Furthermore, we have compared our results to those from a commonly used truncation scheme for FRG equations: the Taylor expansion of the effective potential in powers of $\rho - \rho_0$. In Fig. 6 we again show our full phase diagram calculated on a grid, with an added line (brown, dotted) denoting the result of our Taylor expansion to order ρ^2 . While the transition indeed lies close to the grid result at vanishing imbalance (within $\sim 3\%$), the deviation increases to $\sim 15 - 30\%$ at high $\delta\mu$. This indicates that, even at low imbalance, the impact of higher-order terms in the effective potential is sizeable. At high imbalance, the Taylor expansion eventually breaks down

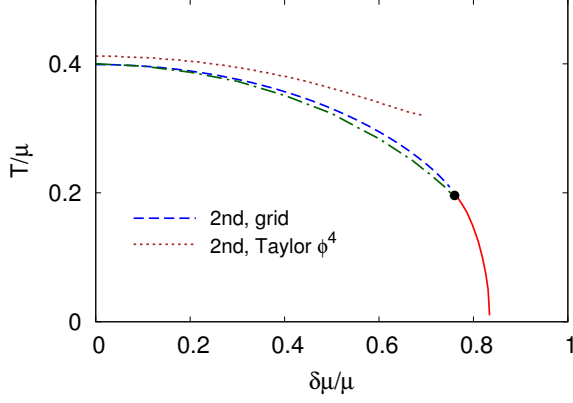


FIG. 6. (Color online) Using a Taylor expansion of the effective average action $U_k(\rho)$ to order $\rho^2 \sim \phi^4$ (brown, dotted line) in the flow equation, the location of the second-order line deviates quantitatively from the grid solution (blue, dashed line) as we increase $\delta\mu/\mu$.

owing to the presence of an additional minimum at the

first-order transition. In this case, the coefficient of ρ^2 can turn negative. Since this is the highest coupling in the system, this entails that the potential becomes unbounded from below, and hence unstable. Taking into account higher orders in the Taylor expansion can extend its domain of applicability. To accurately resolve all minima of the potential, however, very high orders are needed. Alternatively, one can expand about multiple minima separately or use an expansion around a fixed value of ρ , rather than an expansion around the minimum [88]. Interpreting the breakdown of the Taylor expansion as a signal of proximity to the critical point, one would be led to a too low $\delta\mu_{CP}$ as well as too high T_{CP} , at least in this low expansion order. An expansion of the effective average potential to order ϕ^4 has recently been applied to a spin-imbalanced Fermi gas with weak attractive interactions [66]. Accordingly, the superfluid transition was found to be of second order. While the inclusion of higher order terms might diminish the discrepancy in the second-order line to some extent [88], the resolution of the first-order transition is more challenging within a Taylor expansion.

-
- [1] I. Bloch, J. Dalibard, and W. Zwerger, *Rev. Mod. Phys.* **80**, 885 (2008).
 - [2] K. M. O'Hara, S. L. Hemmer, M. E. Gehm, S. R. Granade, and J. E. Thomas, *Science* **298**, 2179 (2002); J. Kinast, S. L. Hemmer, M. E. Gehm, A. Turlapov, and J. E. Thomas, *Phys. Rev. Lett.* **92**, 150402 (2004); J. Kinast, A. Turlapov, J. E. Thomas, Q. Chen, J. Stajic, and K. Levin, *Science* **307**, 1296 (2005).
 - [3] T. Bourdel, J. Cubizolles, L. Khaykovich, K. M. F. Magalhães, S. J. J. M. F. Kokkelmans, G. V. Shlyapnikov, and C. Salomon, *Phys. Rev. Lett.* **91**, 020402 (2003).
 - [4] S. Jochim, M. Bartenstein, A. Altmeyer, G. Hendl, S. Riedl, C. Chin, J. Hecker Denschlag, and R. Grimm, *Science* **302**, 2101 (2003); M. Bartenstein, A. Altmeyer, S. Riedl, S. Jochim, C. Chin, J. H. Denschlag, and R. Grimm, *Phys. Rev. Lett.* **92**, 120401 (2004); C. Chin, M. Bartenstein, A. Altmeyer, S. Riedl, S. Jochim, J. H. Denschlag, and R. Grimm, *Science* **305**, 1128 (2004).
 - [5] C. A. Regal, M. Greiner, and D. S. Jin, *Phys. Rev. Lett.* **92**, 040403 (2004).
 - [6] M. W. Zwierlein, C. A. Stan, C. H. Schunck, S. M. F. Raupach, A. J. Kerman, and W. Ketterle, *Phys. Rev. Lett.* **92**, 120403 (2004); M. W. Zwierlein, J. R. Abo-Shaeer, A. Schirotzek, C. H. Schunck, and W. Ketterle, *Nature (London)* **435**, 1047 (2005).
 - [7] W. Ketterle, D. Durfee, and D. Stamper-Kurn, *Proceedings of the International School of Physics "Enrico Fermi", Course CXL*, edited by M. Inguscio, S. Stringari and C.E. Wieman, 67 (1999).
 - [8] S. Giorgini, L. P. Pitaevskii, and S. Stringari, *Rev. Mod. Phys.* **80**, 1215 (2008).
 - [9] M. W. Zwierlein, A. Schirotzek, C. H. Schunck, and W. Ketterle, *Science* **311**, 492 (2006); M. W. Zwierlein, C. H. Schunck, A. Schirotzek, and W. Ketterle, *Nature (London)* **442**, 54 (2006); Y. Shin, M. W. Zwierlein, C. H. Schunck, A. Schirotzek, and W. Ketterle, *Phys. Rev. Lett.* **97**, 030401 (2006); C. H. Schunck, Y. Shin, A. Schirotzek, M. W. Zwierlein, and W. Ketterle, *Science* **316**, 867 (2007); Y.-I. Shin, C. H. Schunck, A. Schirotzek, and W. Ketterle, *Nature (London)* **451**, 689 (2008).
 - [10] G. B. Partridge, W. Li, R. I. Kamar, Y. A. Liao, and R. G. Hulet, *Science* **311**, 503 (2006); G. B. Partridge, W. Li, Y. A. Liao, R. G. Hulet, M. Haque, and H. T. C. Stoof, *Phys. Rev. Lett.* **97**, 190407 (2006).
 - [11] M. Horikoshi, S. Nakajima, M. Ueda, and T. Mukaiyama, *Science* **327**, 442 (2010).
 - [12] S. Nascimbene, N. Navon, K. J. Jiang, F. Chevy, and C. Salomon, *Nature* **463**, 1057 (2010).
 - [13] M. J. H. Ku, A. T. Sommer, L. W. Cheuk, and M. W. Zwierlein, *Science* **335**, 563 (2012).
 - [14] J. Carlson, S.-Y. Chang, V. Pandharipande, and K. Schmidt, *Phys. Rev. Lett.* **91**, 050401 (2003); G. E. Astrakharchik, J. Boronat, J. Casulleras, and S. Giorgini, *Phys. Rev. Lett.* **93**, 200404 (2004); V. K. Akkineni, D. M. Ceperley, and N. Trivedi, *Phys. Rev. B* **76**, 165116 (2007); A. Bulgac, J. E. Drut, and P. Magierski, *Phys. Rev. Lett.* **96**, 090404 (2006); E. Burovski, N. Prokof'ev, B. Svistunov, and M. Troyer, *Phys. Rev. Lett.* **96**, 160402 (2006); M. Wingate, *PoS LAT2006*, 153 (2006), arXiv:hep-lat/0609054 [hep-lat]; A. Bulgac, J. E. Drut, and P. Magierski, *Phys. Rev. A* **78**, 023625 (2008); J. E. Drut and A. N. Nicholson, *J. Phys. G* **40**, 043101 (2013); O. Goulko and M. Wingate, *Phys. Rev. A* **82**, 053621 (2010).
 - [15] Z. Nussinov and S. Nussinov, *Phys. Rev. A* **74**, 053622 (2006); Y. Nishida and D. T. Son, *Phys. Rev. Lett.* **97**, 050403 (2006); *Phys. Rev. A* **75**, 063617 (2007); P. Arnold, J. E. Drut, and D. T. Son, *Phys. Rev. A* **75**, 043605 (2007); J.-W. Chen and E. Nakano, *Phys.*

- Rev. A **75**, 043620 (2007).
- [16] R. Haussmann, Zeitschrift für Physik B Condensed Matter **91**, 291 (1993); Q. Chen, I. Kosztin, and K. Levin, Phys. Rev. Lett. **85**, 2801 (2000); P. Pieri and G. C. Strinati, Phys. Rev. B **61**, 15370 (2000); A. Perali, P. Pieri, L. Pisani, and G. C. Strinati, Phys. Rev. Lett. **92**, 220404 (2004); P. Pieri, L. Pisani, and G. C. Strinati, Phys. Rev. B **70**, 094508 (2004).
 - [17] S. Diehl and C. Wetterich, Nucl. Phys. **B770**, 206 (2007); Phys. Rev. A **73**, 033615 (2006); R. B. Diener, R. Sensarma, and M. Randeria, Phys. Rev. A **77**, 023626 (2008).
 - [18] M. Y. Veillette, D. E. Sheehy, and L. Radzihovsky, Phys. Rev. A **75**, 043614 (2007).
 - [19] R. Haussmann, W. Rantner, S. Cerrito, and W. Zwerger, Phys. Rev. **A75**, 023610 (2007).
 - [20] M. C. Birse, B. Krippa, J. A. McGovern, and N. R. Walet, Phys. Lett. **B605**, 287 (2005).
 - [21] S. Diehl, H. Gies, J. M. Pawłowski, and C. Wetterich, Phys. Rev. A **76**, 021602 (2007); S. Diehl, H. Gies, J. Pawłowski, and C. Wetterich, Phys. Rev. **A76**, 053627 (2007); P. Nikolić and S. Sachdev, Phys. Rev. A **75**, 033608 (2007); K. B. Gubbels and H. T. C. Stoof, Phys. Rev. Lett. **100**, 140407 (2008); S. Floerchinger, M. Scherer, and C. Wetterich, Phys. Rev. **A81**, 063619 (2010); S. Diehl, S. Floerchinger, H. Gies, J. Pawłowski, and C. Wetterich, Annalen der Physik **522**, 615 (2010); M. M. Scherer, S. Floerchinger, and H. Gies, Phil. Trans. R. Soc. A **368**, 2779 (2011); S. Floerchinger, S. Moroz, and R. Schmidt, Few-Body Systems **51**, 153 (2011).
 - [22] L. Bartosch, P. Kopietz, and A. Ferraz, Phys. Rev. **B80**, 104514 (2009).
 - [23] I. Boettcher, J. M. Pawłowski, and S. Diehl, Nucl. Phys. B - Proc. Suppl. **228**, 63 (2012).
 - [24] N. Kaiser, Nucl. Phys. **A860**, 41 (2011); Eur. Phys. J. **A49**, 140 (2013).
 - [25] T.-L. Ho, Phys. Rev. Lett. **92**, 090402 (2004); S. Tan, Annals of Physics **323**, 2971 (2008); Annals of Physics **323**, 2952 (2008); Annals of Physics **323**, 2987 (2008).
 - [26] F. Chevy, cond-mat/0701350.
 - [27] C. Lobo, A. Recati, S. Giorgini, and S. Stringari, Phys. Rev. Lett. **97**, 200403 (2006).
 - [28] F. Chevy, Phys. Rev. A **74**, 063628 (2006).
 - [29] R. Combescot, A. Recati, C. Lobo, and F. Chevy, Phys. Rev. Lett. **98**, 180402 (2007).
 - [30] A. Bulgac and M. M. Forbes, Phys. Rev. A **75**, 031605 (2007).
 - [31] N. Prokof'ev and B. Svistunov, Phys. Rev. B **77**, 020408 (2008).
 - [32] S. Pilati and S. Giorgini, Phys. Rev. Lett. **100**, 030401 (2008).
 - [33] R. Schmidt and T. Enss, Phys. Rev. A **83**, 063620 (2011).
 - [34] A. M. Clogston, Phys. Rev. Lett. **9**, 266 (1962).
 - [35] B. S. Chandrasekhar, Applied Physics Letters **1** (1962).
 - [36] D. E. Sheehy and L. Radzihovsky, Phys. Rev. Lett. **96**, 060401 (2006).
 - [37] K. Gubbels, M. Romans, and H. Stoof, Phys. Rev. Lett. **97**, 210402 (2006).
 - [38] M. M. Parish, F. M. Marchetti, A. Lamacraft, and B. D. Simons, Nature Physics **3**, 124 (2007).
 - [39] G. Sarma, Journal of Physics and Chemistry of Solids **24**, 1029 (1963).
 - [40] I. Boettcher, T. Herbst, J. Pawłowski, N. Strodthoff, L. von Smekal, and C. Wetterich, (2014), arXiv:1409.5232 [cond-mat.quant-gas].
 - [41] P. Fulde and R. A. Ferrell, Phys. Rev. **135**, A550 (1964).
 - [42] A. Larkin and Y. Ovchinnikov, Zh. Eksp. Teor. Fiz. **47**, 1136 (1964).
 - [43] J. Braun, J.-W. Chen, J. Deng, J. E. Drut, B. Friman, et al., Phys. Rev. Lett. **110**, 130404 (2013).
 - [44] D. Roscher, J. Braun, J.-W. Chen, and J. E. Drut, J. Phys. **G41**, 055110 (2014).
 - [45] J. Braun, J. E. Drut, and D. Roscher, (2014), arXiv:1407.2924 [cond-mat.quant-gas].
 - [46] V. Gurarie and L. Radzihovsky, Annals of Physics **322**, 2 (2007).
 - [47] G. Zürn, T. Lompe, A. N. Wenz, S. Jochim, P. S. Julienne, and J. M. Hutson, Phys. Rev. Lett. **110**, 135301 (2013).
 - [48] J. W. Negele and H. Orland, *Quantum Many-Particle Systems* (Westview Press, 1998).
 - [49] A. Altland and B. Simons, *Condensed Matter Field Theory* (Cambridge University Press, 2010).
 - [50] H. T. C. Stoof, K. B. Gubbels, and D. B. M. Dickerscheid, *Ultracold Quantum Fields* (Springer, Dordrecht, 2009).
 - [51] J. E. Baarsma, K. B. Gubbels, and H. T. C. Stoof, Phys. Rev. A **82**, 013624 (2010).
 - [52] F. Chevy and C. Mora, Rept. Prog. Phys. **73**, 112401 (2010).
 - [53] K. Gubbels and H. Stoof, Phys. Rept. **525**, 255 (2013).
 - [54] D. F. Litim and J. M. Pawłowski, World Sci. , 168 (1999), arXiv:hep-th/9901063; J. Berges, N. Tetradis, and C. Wetterich, Phys. Rept. **363**, 223 (2002); H. Gies, Lect. Notes Phys. **852**, 287 (2012); B.-J. Schaefer and J. Wambach, Phys. Part. Nucl. **39**, 1025 (2008); J. M. Pawłowski, Annals of Physics **322**, 2831 (2007); B. Delamotte, Lect. Notes Phys. **852**, 49 (2012); P. Kopietz, L. Bartosch, and F. Schütz, *Introduction to the Functional Renormalization Group* (Springer, Berlin, 2010); W. Metzner, M. Salmhofer, C. Honerkamp, V. Meden, and K. Schonhammer, Rev. Mod. Phys. **84**, 299 (2012); J. Braun, J. Phys. **G39**, 033001 (2012); L. von Smekal, Nucl. Phys. Proc. Suppl. **228**, 179 (2012), arXiv:1205.4205 [hep-ph].
 - [55] J.-P. Blaizot, arXiv:0801.0009 [cond-mat.stat-mech].
 - [56] C. Wetterich, Physics Letters B **301**, 90 (1993).
 - [57] I. Boettcher, J. M. Pawłowski, and C. Wetterich, Phys. Rev. A **89**, 053630 (2014).
 - [58] N. Dupuis and K. Sengupta, EPL **80**, 50007 (2007).
 - [59] C. Wetterich, Phys. Rev. B **77**, 064504 (2008).
 - [60] P. Strack, R. Gersch, and W. Metzner, Phys. Rev. B **78**, 014522 (2008).
 - [61] A. Eberlein and W. Metzner, Phys. Rev. B **89**, 035126 (2014).
 - [62] D. Schnoerr, I. Boettcher, J. M. Pawłowski, and C. Wetterich, Annals Phys. **334**, 83 (2013).
 - [63] H. C. Krah, S. Friederich, and C. Wetterich, Phys. Rev. B **80**, 014436 (2009).
 - [64] J. Braun and D. Roscher, in preparation (2014).
 - [65] N. Navon, S. Nascimbène, X. Leyronas, F. Chevy, and C. Salomon, Phys. Rev. A **88**, 063614 (2013).
 - [66] B. Krippa, (2014), arXiv:1407.5438 [cond-mat.quant-gas].
 - [67] P. Strack and P. Jakubczyk, Phys. Rev. X **4**, 021012 (2014).
 - [68] J. Braun, Phys. Rev. **D81**, 016008 (2010).
 - [69] C. A. R. Sá de Melo, M. Randeria, and J. R. Engelbrecht,

- Phys. Rev. Lett. **71**, 3202 (1993).
- [70] M. Randeria and N. Trivedi, Journal of Physics and Chemistry of Solids **59**, 1754 (1998).
 - [71] J. P. Gaebler, J. T. Stewart, T. E. Drake, D. S. Jin, A. Perali, P. Pieri, and G. C. Strinati, Nature Physics **6**, 569 (2010).
 - [72] A. Perali, F. Palestini, P. Pieri, G. C. Strinati, J. T. Stewart, J. P. Gaebler, T. E. Drake, and D. S. Jin, Phys. Rev. Lett. **106**, 060402 (2011).
 - [73] E. Mueller, Phys. Rev. A **83**, 053623 (2011).
 - [74] Y. Sagi, T. E. Drake, R. Paudel, R. Chapurin, and D. S. Jin, (2014), arXiv:1409.4743 [cond-mat.quant-gas].
 - [75] S. Tsuchiya, R. Watanabe, and Y. Ohashi, Phys. Rev. A **80**, 033613 (2009).
 - [76] R. Watanabe, S. Tsuchiya, and Y. Ohashi, Phys. Rev. A **82**, 043630 (2010).
 - [77] D. F. Litim, J. M. Pawłowski, and L. Vergara, (2006), arXiv:hep-th/0602140 [hep-th].
 - [78] A. Ringwald and C. Wetterich, Nucl. Phys. **B334**, 506 (1990).
 - [79] A. Recati, C. Lobo, and S. Stringari, Phys. Rev. A **78**, 023633 (2008).
 - [80] M. Ku, J. Braun, and A. Schwenk, Phys. Rev. Lett. **102**, 255301 (2009).
 - [81] J. Braun, J. E. Drut, T. Jahn, M. Pospiech, and D. Roscher, Phys. Rev. **A89**, 053613 (2014).
 - [82] J. Braun, B. Klein, and H. Pirner, Phys. Rev. **D72**, 034017 (2005).
 - [83] J. Braun, S. Diehl, and M. M. Scherer, Phys. Rev. A **84**, 063616 (2011).
 - [84] J. Braun, B. Klein, and B.-J. Schaefer, Phys. Lett. **B713**, 216 (2012).
 - [85] A. Bulgac and M. M. Forbes, Phys. Rev. Lett. **101**, 215301 (2008).
 - [86] J. E. Baarsma and H. T. C. Stoof, (2012), arXiv:1212.5450 [cond-mat.quant-gas].
 - [87] L. Radzihovsky, Physica C: Superconductivity **481**, 189 (2012).
 - [88] J. M. Pawłowski and F. Rennecke, Phys. Rev. D **90**, 076002 (2014).